RSC Advances

PAPER

View Article Online
View Journal | View Issue

Check for updates

Cite this: *RSC Adv.*, 2020, **10**, 40948

# A study on the selective catalytic reduction of $NO_x$ by ammonia on sulphated iron-based catalysts

Caixia Liu, *[a] Huijun Wang,[a] Yalian Bi[a] and Ziyin Zhang[b]

A series of sulphated iron-based catalysts was prepared *via* an impregnation method by changing the loading content of $Fe^{3+}$ and $SO_4^{2-}$ on $ZrO_2$, and their performance in the selective catalytic reduction (SCR) of $NO_x$ by ammonia was investigated. The $NO_x$ conversion exhibited large differences among the sulphated iron-based catalysts. To explore the synergistic mechanism of iron and sulphates, XRD, BET, $H_2$-TPR, XPS, TPD and *in situ* DRIFTS were used to characterize the catalysts, and it was found that among all the catalysts, the $NO_x$ conversion by $Fe_2SZr$ was greater than 90% at 350–450 °C. The results indicated that the interaction between $Fe^{3+}$ and $SO_4^{2-}$ can have an effect on the redox ability, acid sites, and adsorption of $NO_x$ and $NH_3$. With an increase in the content of $Fe^{3+}$, the redox activity of the catalyst and the adsorption of ammonia improved at medium and low temperatures. However, at higher temperatures, an increase in $Fe^{3+}$ led to a decrease in the conversion of $NO_x$ due to the enhanced oxidation of $NH_3$. At medium and low temperatures, an increase in the content of $SO_4^{2-}$ decreased the concentration of $Fe^{3+}$ on the surface of the catalyst and inhibited the adsorption of $NO_x$ and $NH_3$. The addition of $SO_4^{2-}$ reduced the redox activity of the catalyst and inhibited the oxidation reaction of $NH_3$, which follows the Eley–Rideal mechanism at high temperatures, further enhancing the SCR activity of the $Fe_xS_yZr$ catalyst.

Received 3rd August 2020
Accepted 8th October 2020

DOI: 10.1039/d0ra06697d

rsc.li/rsc-advances

Open Access Article. Published on 10 Novemba 2020. Downloaded on 27/04/2026 23:59:39.
This article is licensed under a Creative Commons Attribution-NonCommercial 3.0 Unported Licence.

## 1. Introduction

The temperature of the waste gas of a bituminous coal-fired power plant is generally 300–450 °C.[1,2] In particular, the temperature after burning lignite reaches up to 420 °C. Also, under conditions with a high sulphur content, the commercially available catalysts (vanadium-based catalysts) show low denitrification activity and poor $N_2$ selectivity, which make them easily poisoned and secondary pollution being released into the environment.[3–6] Therefore, it is urgent to develop environment-friendly catalysts with sulphur resistance, high activity, and high $N_2$ selectivity at high temperature.[7–9]

Iron-based catalysts exhibit a good $NO_x$ conversion rate and $N_2$ selectivity, and thus, have been favored by many researchers.[10–17] However, the selective catalytic reduction (SCR) activity of $\alpha$-$Fe_2O_3$ catalysts at temperatures above 300 °C significantly decreases, and thus they cannot be applied in the denitrification of waste gas after burning coal. In recent years, some researchers attempted to improve the performance of catalysts by sulphating them. Gu *et al.*[18] carried out the sulphation of $CeO_2$ *via* a gas phase method, achieving a reaction activity of up to 99% in the temperature range of 300–500 °C. Ma *et al.*[19] prepared $Fe_2(SO_4)_3/TiO_2$ *via* impregnation, exhibiting a conversion rate of 97% and $N_2O$ selectivity lower than 5% at 350–450 °C. Therefore, the sulphation of catalysts is a very effective way to improve their reactivity and $N_2$ selectivity at high temperature. According the literature,[20–25] the high catalytic efficiency and good sulfur resistance of catalysts upon acidification treatment can be mainly ascribed to the following reasons: (1) the reaction with the active material improves the transformation between the active material ion, increasing the reaction rate. (2) The number of Brönsted acid sites on the surface of the catalyst increases, increasing the strength of the acid sites, which is the main reason for the increase in catalytic activity. (3) Reaction with other substances on the catalyst to form sulfates, which enclose the active substances and reduce the sulphation of the active substances or act as active substances. Importantly, the $NO_x$ conversion efficiency and $N_2$ selectivity of the sulphated catalysts improved.

To date, the synergistic mechanism between the active components and sulphates has not been reported. Therefore, we used Fe as an active component, which was sulphated and loaded onto a $ZrO_2$ carrier, to prepare a catalyst with a high $NO_x$ conversion rate and high $N_2$ selectivity at high temperature. In this study, we loaded $Fe^{3+}$ and $SO_4^{2-}$ in different amounts on the $ZrO_2$ carrier *via* the impregnation method. The impact of $Fe^{3+}$ and $SO_4^{2-}$ loading on the performance of the $NH_3$-SCR catalyst was investigated using different characterization methods, and the synergistic mechanism of $Fe^{3+}$ and $SO_4^{2-}$ in the SCR reaction was discussed.

[a]*School of Environmental Science and Engineering, Tianjin University, Tianjin 300072, China. E-mail: liucx@tju.edu.cn; Fax: +86-22-8740-2075; Tel: +86-13426103078*
[b]*Langfang City Beichen Entrepreneurship Resin Materials Incorporated Company, Langfang 065000, China. E-mail: laowuzhangziyin@163.com; Tel: +86-15010892987*


This journal is © The Royal Society of Chemistry 2020

Open Access Article. Published on 10 Novemba 2020. Downloaded on 27/04/2026 23:59:39.
This article is licensed under a Creative Commons Attribution-NonCommercial 3.0 Unported Licence.

## 2. Experimental

### 2.1 Catalyst preparation

All catalysts were prepared *via* the incipient wetness method. $ZrO_2$ power was weighed and dissolved in deionized water. Subsequently, $Fe(NO_3)_3 \cdot 9H_2O$ and $(NH_4)_2SO_4$ were added to the solution dropwise, and then heated to 70 °C and stirred to form a paste. The resulting mixture was dried at 120 °C overnight and calcined in air at 500 °C for 4 h. Finally, a series of iron-based catalysts was obtained, denoted as $Fe_xS_yZr$ ($y = 5$, $x = 0$, 2, 3.5, 7 is denoted as $Fe_xSZr$ and $x = 3.5$, $y = 0$, 5, 10, 15 is denoted as $FeS_yZr$; where $x$ represents the weight percentage of $Fe^{3+}$ and $y$ represents the weight percentage of $SO_4^{2-}$).

### 2.2 Catalyst characterization

The gas concentration was detected using a Gasmet Dx-4000 FT-IR gas analyser, which can monitor $NH_3$, $NO_2$, NO, $N_2O$ and water vapour. The reactant gas was 500 ppm $NH_3$, 500 ppm NO, 3% $O_2$ and $N_2$ balanced.

X-ray diffraction (XRD) measurements were performed on a D/MAX-RB system with Cu Ka radiation. The diffraction curves were measured in the $2\theta$ range 10° to 90° with a step size of 0.018 at a rate of 1 s per step.

BET measurements were performed using a Quantachrome Autosorb AS-1 System using $N_2$ adsorption at 77 K.

X-ray photoelectron spectroscopy (XPS) was performed using an ESCALab220i-XL electron spectrometer with 300 W Mg Ka radiation under $3 \times 10^{-9}$ mbar. The binding energies were calibrated using adventitious carbon with C 1s at 284.8 eV.

Temperature-programmed reduction (TPR) curves were measured using a Micromeritics ChemiSorb 2720. Firstly, the samples were preheated to 300 °C and maintained at a constant temperature for 1 h under $N_2$ purging and then cooled to 30 °C. The catalysts were reduced in a flow of $N_2$-based gas containing 10% $H_2$/Ar (50 $cm^3$ $min^{-1}$), and the temperature was programmed from 30 °C to 1000 °C at a heating rate of 10 °C $min^{-1}$.

Temperature programmed desorption ($NH_3$-TPD) experiments were conducted in an $N_2$-based mixture gas containing 500 ppm $NH_3$ (300 mL $min^{-1}$). The sample was preheated at 500 °C constantly for 1 h, then cooled to 30 °C, and $NH_3$ was introduced continuously for 1 h. Thirdly, the catalyst was blown with $N_2$ until to no $NH_3$ was detected. Finally, the catalyst was heated from 30 °C to 500 °C at a heating rate of 10 °C $min^{-1}$.

*In situ* DRIFTS spectra were characterized using a Nicolet NEXUS 870 FT-IR spectrometer. The sample was pre-treated at 300 °C for 1 h under a flow of $N_2$ (100 $cm^3$ $min^{-1}$).

## 3. Results and discussion

### 3.1 The effects on SCR activity with different loadings of $Fe^{3+}$ and $SO_4^{2-}$

Fig. 1(a) shows the SCR activities of the SZr, $Fe_2SZr$, $Fe_{3.5}SZr$ and $Fe_7SZr$ catalysts. According to this figure, the $NO_x$ conversions of $S_5Zr$ catalyst were very low in the temperature range of 150–500 °C and it reached the highest of 12% at 500 °C. Upon the addition of 2% $Fe^{3+}$, the $NO_x$ conversions improved significantly, climbing rapidly from 10% at 250 °C to 90% at 350 °C, and reached the highest of 98% at 400 °C. Subsequently, with a further increase in the temperature to 500 °C, the $NO_x$ conversion decreased to 57%. With a continuous increase in the loading of $Fe^{3+}$, the $NO_x$ conversions were slightly higher than that of the $Fe_2SZr$ catalyst in the temperature range of 250–350 °C, but they dropped significantly in the temperature range of 400–500 °C, which was negative at 500 °C.

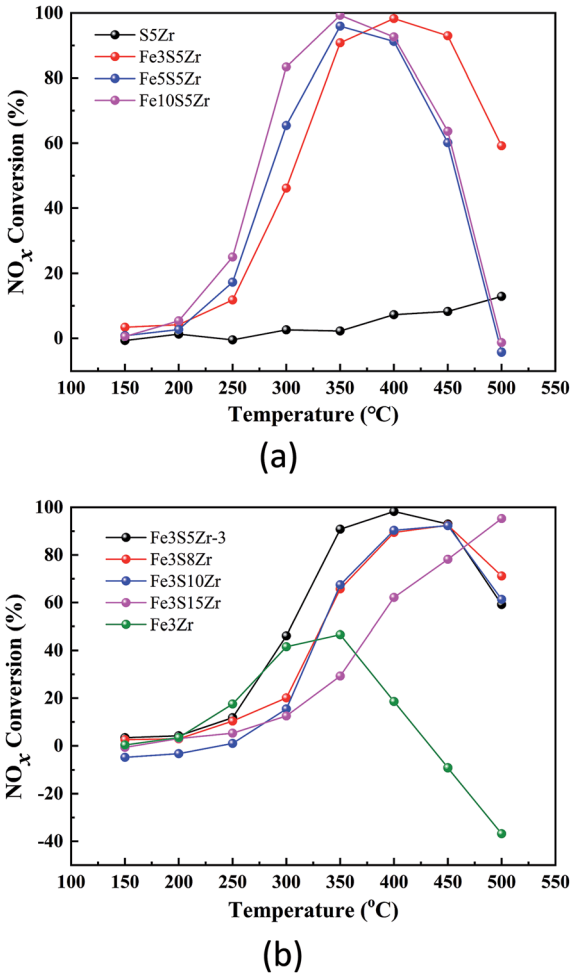


Fig. 1 (a) $NO_x$ conversion of catalysts containing 5% $SO_4^{2-}$ and $x$% $Fe^{3+}$ ($x = 0$, 2, 3.5, 7). (b) $NO_x$ conversion of catalysts containing 3.5% $Fe^{3+}$ and $y$% $SO_4^{2-}$ ($y = 0$, 5, 10, 15).

Fig. 1(b) shows the $NO_x$ conversions by the FeZr, $FeS_5Zr$, $FeS_{10}Zr$ and $FeS_{15}Zr$ catalysts in the temperature range of 150–500 °C. According to this figure, the $NO_x$ conversions of the FeZr, $FeS_5Zr$ and $FeS_{10}Zr$ catalysts increased initially and then declined in the temperature range of 150–500 °C. The $NO_x$ conversions of the FeZr catalyst were very close to that of the $FeS_5Zr$ catalyst in the temperature range of 150–300 °C, which reached the peak of 46% at 350 °C, and then dropped sharply to a negative value from 400 °C to 500 °C. Upon the loading of $SO_4^{2-}$, the $NO_x$ conversions improved in the high temperature range. When 10% $SO_4^{2-}$ was added to the catalyst, the $NO_x$ conversions were reduced in the temperature range of 250–450 °C compared with that of the $FeS_5Zr$ catalyst. With the

Open Access Article. Published on 10 Novemba 2020. Downloaded on 27/04/2026 23:59:39.
This article is licensed under a Creative Commons Attribution-NonCommercial 3.0 Unported Licence.

further addition of $SO_4^{2-}$ to 15%, the $NO_x$ conversion exhibited an increasing trend from 150 °C to 500 °C, which was much lower than that of the $FeS_5Zr$ catalyst in the range of 150–450 °C but it reached close to 100% at 500 °C.

### 3.2 Impact of $Fe^{3+}$ and $SO_4^{2-}$ loading on ammonia oxidation

Fig. 2(a) shows the curve of ammonia oxidation using a series of acidified catalysts in the temperature range of 150–500 °C. Accordingly, the SZr catalyst without $Fe^{3+}$ loading started to oxidize $NH_3$ beginning at 400 °C and reached an $NH_3$ oxidation rate of 40% at 500 °C. However, it was reported that the self-oxidation reaction of $NH_3$ occurs when the temperature is higher than 400 °C, and thus, we speculated that a self-oxidation reaction mainly occurred on the SZr catalyst. With an increase in the loading amount of $Fe^{3+}$, the conversion of $NH_3$ oxidation shifted to a lower temperature, that is, the greater the loading amount of $Fe^{3+}$, the more the starting temperature of $NH_3$ oxidation was shifted to a lower temperature and the higher the corresponding oxidation rate of $NH_3$ in the temperature range of 300–450 °C. However, the $NH_3$ oxidation rates of the $Fe_{3.5}SZr$ and $Fe_7SZr$ catalysts were close, indicating that although the higher the loading amount of $Fe^{3+}$, the higher the $NH_3$ oxidation rate, the $NH_3$ oxidation rate approached a constant at a certain temperature with a continuous increase in $Fe^{3+}$. In general, an increase in the amount of $Fe^{3+}$ will promote the oxidation of $NH_3$ at high temperature. Combining the activities of the catalysts with varying amounts of $Fe^{3+}$, the $NH_3$ self-oxidation reaction mainly occurred on the $Fe_2SZr$, $Fe_{3.5}SZr$ and $Fe_7SZr$ catalysts at 450–500 °C, which affected the efficiency of the catalytic reduction of the nitrogen oxides. Fig. 2(b) shows the changes in the curves of the $NH_3$ oxidation rate with the catalysts prepared by changing the content of sulphates. Accordingly, for the FeZr catalyst in the absence of sulphates, the oxidation reaction of $NH_3$ started from 250 °C, and the $NH_3$ oxidation rate reached 80% at 350 °C, while it reached 100% at 400 °C. Thus, based on the curve of the $NH_3$ oxidation rate for the FeZr catalyst, it can be concluded that in the temperature range of 350–500 °C, the $NH_3$ oxidation reaction mainly occurred on the FeZr catalyst, thus affecting the SCR reaction. With an increase in the sulphate content, the most efficient ammonia oxidation shifted to a higher temperature, that is, the addition of sulphates inhibited the oxidation reaction of $NH_3$ on the catalyst.

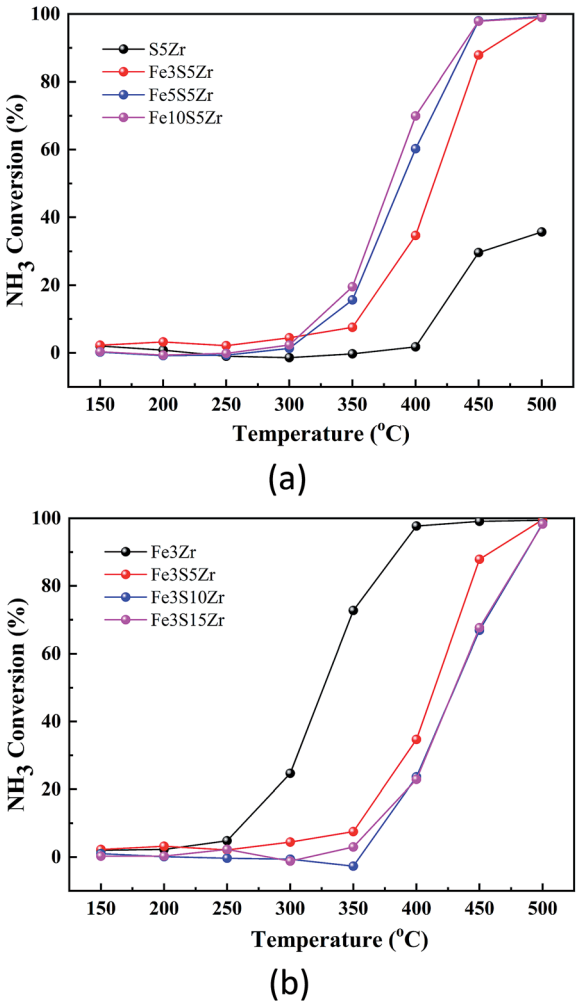


Fig. 2 (a) $NH_3$ oxidation efficiency of catalysts containing 5% $SO_4^{2-}$ and $x$% $Fe^{3+}$ ($x$ = 0, 2, 3.5, 7). (b) The $NH_3$ oxidation efficiency of catalysts containing 3.5% $Fe^{3+}$ and $y$% $SO_4^{2-}$ ($y$ = 0, 5, 10, 15).

### 3.3 $H_2$-temperature programmed reduction (TPR) analysis

The redox ability of catalysts is of great importance for the SCR reaction, which can be well characterized by $H_2$-temperature programmed reduction (TPR). Actually, the lower the temperature, the better the redox ability of the catalyst at low or medium temperatures.[26] The amount of hydrogen consumption is also an important indicator of the catalytic activity. The greater the hydrogen consumption, the stronger the redox capacity of the catalyst.[26–28] As shown in Fig. 3(a), there is only one $H_2$ reduction peak for the SZr catalyst at 583 °C, which is mainly attributed to the reduction peak of the sulphate species. According to the $H_2$-TPR curves of the series of $Fe_2SZr$ catalysts, the reduction temperatures of the catalysts after the addition of $Fe^{3+}$ were lower than that of SZr. The $Fe_{3.5}SZr$ and $Fe_2SZr$ catalysts each showed only one redox peak, and these peaks were close to each other at 471 °C and 443 °C. These two reduction peaks are considered to be the completely overlapping reduction peaks of the iron oxide and the sulphates. The $H_2$-TPR redox curve of the $Fe_7SZr$ catalyst has two reduction peaks at 425 °C and 473 °C. The former reduction peak can be attributed to the reduction peak of the iron oxide, while the peak at 473 °C is considered to be the overlapping reduction peaks of the iron oxide and the sulphates. As shown in Fig. 3(b), the $H_2$-TPR curve of the FeZr catalyst mainly has three reduction peaks at 330 °C and 410 °C, which can be attributed to the reduction peaks of $Fe_2O_3$–$Fe_3O_4$–Fe.[19] After the addition of $SO_4^{2-}$, the reduction temperatures of the catalysts are higher than that of FeZr. The $FeS_{10}Zr$ catalyst has only one reduction peak at 519 °C, which is close to the reduction peak of the SZr catalyst, and it is also considered to be the overlapping reduction peaks of the iron oxide and sulphates. The $H_2$-TPR redox curve of the $FeS_{15}Zr$ catalyst has

 This journal is © The Royal Society of Chemistry 2020

Open Access Article. Published on 10 Novemba 2020. Downloaded on 27/04/2026 23:59:39.
This article is licensed under a Creative Commons Attribution-NonCommercial 3.0 Unported Licence.

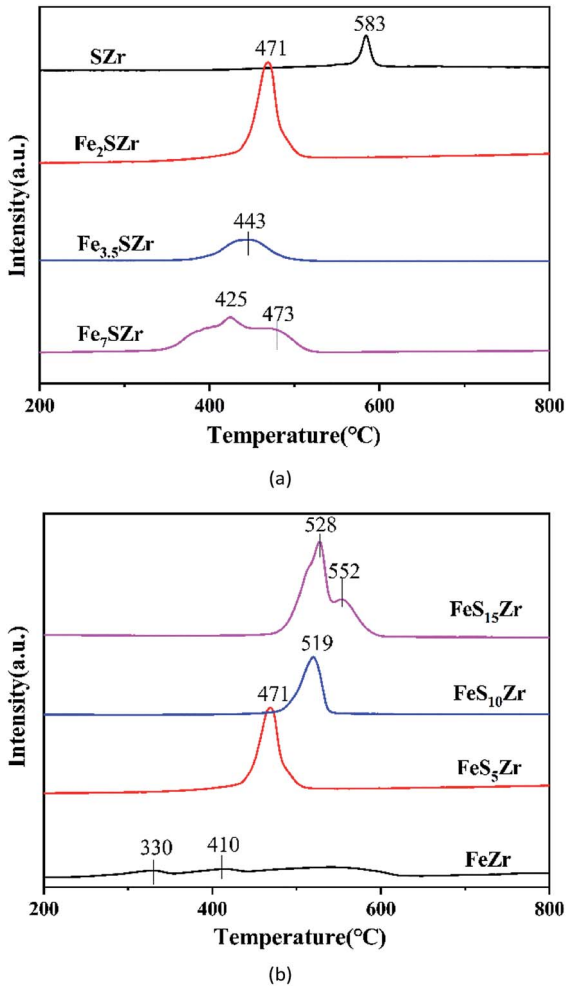


Fig. 3 (a) $H_2$-TPR of catalysts containing 5% $SO_4^{2-}$ and $x$% $Fe^{3+}$ ($x$ = 0, 2, 3.5, 7). (b) $H_2$-TPR of catalysts containing 3.5% $Fe^{3+}$ and $y$% $SO_4^{2-}$ ($y$ = 0, 5, 10, 15).

two reduction peaks at 528 °C and 552 °C. The former reduction peak can be attributed to the reduction peak of the iron oxide, while that at 552 °C is considered to be the overlapping reduction peaks of iron oxide and sulphates. According to Fig. 3, it can be concluded that the increase in the $Fe^{3+}$ content in the catalyst caused a shift in the starting reduction temperature of the catalyst to a lower temperature, indicating that an increase in the content of $Fe^{3+}$ increased the redox activity of the catalyst, and the addition of $SO_4^{2-}$ caused the starting reduction temperature of the catalyst to shift to a higher temperature, indicating that the addition of $SO_4^{2-}$ significantly reduced the redox activity of the catalyst.

### 3.4 XPS

Table 1 shows the atomic concentrations of S, O, Fe and Zr on the surfaces of the different catalysts. Accordingly, when the content of $Fe^{3+}$ was constant, with an increase in $SO_4^{2-}$, the concentration of Fe atoms on the surface showed a decreasing trend. This is mainly due to the formation of $Fe_2(SO_4)_3$. When the content of $SO_4^{2-}$ was constant, with an increase in $Fe_2O_3$, the concentration of S atoms on the surface of the catalyst

Table 1 The surface element content in the different catalysts (%)

| | FeZr | $FeS_5Zr$ | $FeS_{10}Zr$ | $FeS_{15}Zr$ | SZr | $Fe_{3.5}SZr$ | $Fe_7SZr$ |
|---|---|---|---|---|---|---|---|
| S 2p | 0.000 | 0.077 | 0.076 | 0.091 | 0.062 | 0.080 | 0.066 |
| Zr 3d | 0.217 | 0.161 | 0.184 | 0.164 | 0.212 | 0.132 | 0.131 |
| O 1s | 0.698 | 0.719 | 0.722 | 0.723 | 0.726 | 0.695 | 0.690 |
| Fe 2p | 0.074 | 0.045 | 0.018 | 0.021 | 0.000 | 0.093 | 0.113 |

increased initially, and then decreased. Similarly, we concluded that more $Fe_2(SO_4)_3$ was produced so that the Fe and S atoms were enriched on the surface. However, when the content of $Fe^{3+}$ increased to a certain level, the $SO_4^{2-}$ on the surface was covered by $Fe^{3+}$, and thus, the concentration of S atoms on the surface of the catalyst showed the tendency to increase initially, and then decrease with an increase in $Fe^{3+}$.

The oxidation states of Fe and S on the different catalysts were characterized using XPS, and the results are shown in Fig. 4. The Fe 2p and S bands in Fig. 4 were deconvoluted by searching for the optimal combination with correlation coefficients ($R^2$) above 0.99 (Origin Pro 8.0). From the curves of Fe 2p, as shown in Fig. 4(a and b), the bonding energies of Fe $2p_{3/2}$ (710–711.5 eV) and Fe $2p_{1/2}$ (724.3–725.5 eV) corresponded well to the references,[29] and the bonding energies of 718.1–719.2 eV corresponded well to the fingerprint peak of $Fe^{3+}$. Specially, when the content of $SO_4^{2-}$ was 5%, with an increase in $Fe^{3+}$, the peak with a binding energy at 718.1–719.2 eV became strong, and when the $Fe^{3+}$ content was 3.5%, with an increase in $SO_4^{2-}$, the peak at 718.1–719.2 eV became weak.

The S 2p XPS spectra for the different catalysts are shown in Fig. 4(c and d). The S 2p XPS spectra of the sulfated catalysts exhibited a main peak at 168.8–170 eV, as shown in Fig. 4. This value is consistent with $S^{6+}$ such as sulfur in $SO_4^{2-}$,[19] indicating that S is in the $S^{6+}$ oxidation state on the catalyst.

### 3.5 $NH_3$-temperature programmed desorption (TPD) analysis

The acidity of catalysts plays a very important role in the SCR reaction, and $Fe^{3+}$ and sulphates can provide acidic sites, which can improve the acidity of the catalyst. Therefore, the characteristics of $NH_3$-TPD were analysed for a series of acidified catalysts, as shown in Fig. 5. Fig. 5(a) shows the $NH_3$-TPD curves for the catalysts with different $Fe^{3+}$ loadings. The SZr catalyst has two desorption peaks at 410 °C and 120 °C. The desorption amount of ammonia at high temperature was much larger than that at low temperature. It has been reported that the desorption at low temperature is mainly physical adsorption or weak chemical adsorption, while the desorption at high temperature is mainly the strong chemical adsorption of $NH_3$.[30–32] On the $Fe_2SZr$ catalyst, there was a wide $NH_3$ desorption peak in the range of 80 °C to 500 °C. With the addition of $Fe^{3+}$, the desorption capacity of $Fe_{3.5}SZr$ at low temperature (90–180 °C) was slightly higher than the desorption at high temperature (>180 °C). Compared to SZr, the desorption peak of the $Fe_7SZr$ catalyst at high temperature (240 °C) shifted to a lower temperature at nearly 170 °C. Thus, it can be concluded that the

Open Access Article. Published on 10 Novemba 2020. Downloaded on 27/04/2026 23:59:39.
This article is licensed under a Creative Commons Attribution-NonCommercial 3.0 Unported Licence.

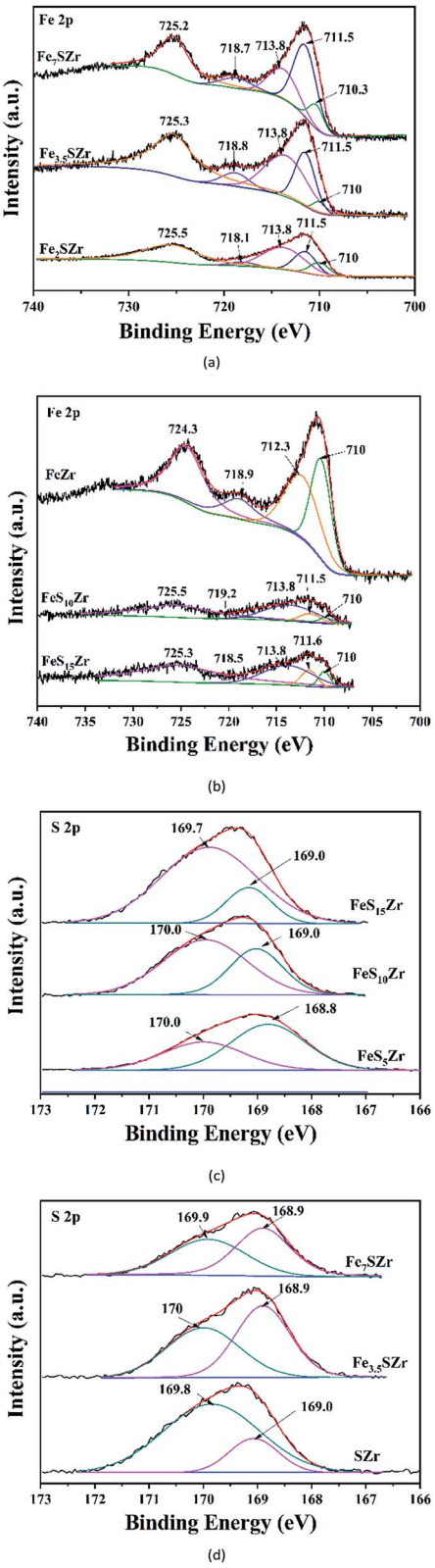


Fig. 4 XPS spectra of different catalysts: (a) XPS-Fe 2p spectra of catalysts containing 5% $SO_4^{2-}$ and $x$% $Fe^{3+}$ ($x$ = 0, 2, 3.5, 7). (b) XPS-Fe 2p spectra of catalysts containing 3.5% $Fe^{3+}$ and $y$% $SO_4^{2-}$ ($y$ = 0, 5, 10, 15). (c) XPS-S 2p spectra of catalysts containing 5% $SO_4^{2-}$ and $x$% $Fe^{3+}$ ($x$ = 0, 2, 3.5, 7). (d) XPS-S 2p spectra of catalysts containing 3.5% $Fe^{3+}$ and $y$% $SO_4^{2-}$ ($y$ = 0, 5, 10, 15).

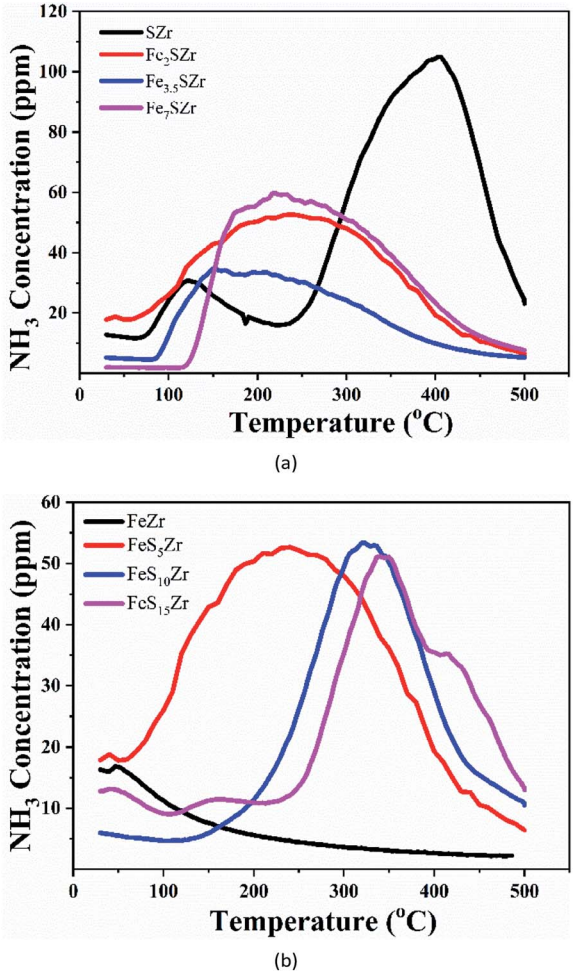


Fig. 5 (a) $NH_3$-TPD of catalysts containing 5% $SO_4^{2-}$ and $x$% $Fe^{3+}$ ($x$ = 0, 2, 3.5, 7). (b) $NH_3$-TPD of catalysts containing 3.5% $Fe^{3+}$ and $y$% $SO_4^{2-}$ ($y$ = 0, 5, 10, 15).

addition of $Fe_2O_3$ reduced the ability of the catalyst to adsorb ammonia at high temperatures and improved the ability of the catalyst to adsorb ammonia at moderate and low temperatures. Fig. 5(b) shows the $NH_3$-TPD curves for the catalysts with different amounts of sulphates. As shown, only a small amount of physically adsorbed ammonia was released on the FeZr catalyst. The addition of 5% sulphate greatly increased the adsorption amount of $NH_3$. With an increase in the amount of sulphate, the desorption peak of ammonia obviously shifted towards a higher temperature, and the $FeS_{15}Zr$ catalyst showed a desorption peak at 410 °C, which is consistent with the desorption peak of the SZr catalyst, but the desorption amount of ammonia was much less than that of the SZr catalyst. Thus, the addition of $SO_4^{2-}$ increased the adsorption of ammonia on the catalyst at high temperatures and reduced the amount of ammonia adsorbed by the catalyst at moderate or low temperatures.

### 3.6 NO + $O_2$-TPD

Fig. 6 shows the $NO_x$-TPD curve for a series of acidified catalysts. As shown in Fig. 6(a), the SZr catalyst mainly has a nitrogen

 This journal is © The Royal Society of Chemistry 2020

Open Access Article. Published on 10 Novemba 2020. Downloaded on 27/04/2026 23:59:39.
This article is licensed under a Creative Commons Attribution-NonCommercial 3.0 Unported Licence.

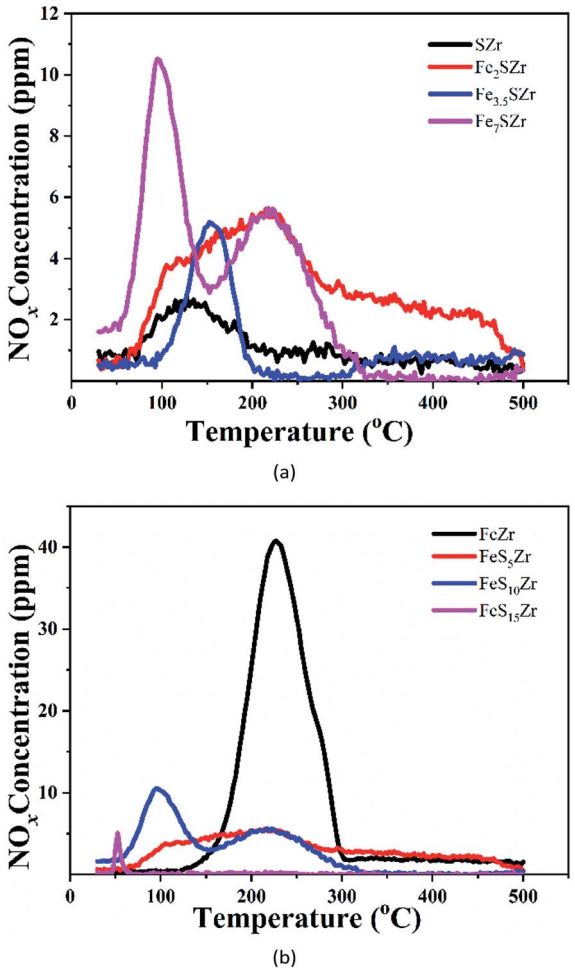


Fig. 6 (a) NO + $O_2$-TPD of catalysts containing 5% $SO_4^{2-}$ and $x$% $Fe^{3+}$ ($x = 0$, 2, 3.5, 7). (b) The NO + $O_2$-TPD of catalysts containing 3.5% $Fe^{3+}$ and $y$% $SO_4^{2-}$ ($y = 0$, 5, 10, 15).

oxide desorption peak at 120 °C with a low desorption amount. After the addition of 2% $Fe^{3+}$, nitrogen oxides were desorbed from 100 °C to 500 °C, and the amount of nitrogen oxides desorbed was greatly enhanced. When the addition of $Fe^{3+}$ reached 3.5%, the desorption peak shifted to a higher temperature by approximately 40 °C, but the desorption amount was significantly reduced. When the addition of $Fe^{3+}$ reached 7%, two desorption peaks at 90 °C and 230 °C existed, and the desorption amount was greater than that of the $Fe_2SZr$ catalyst. As shown in Fig. 6(b), the FeZr catalyst has a nitrogen oxide desorption peak at 240 °C with the highest amount of desorption. The addition of 5% $SO_4^{2-}$ to the catalyst significantly decreased the desorption of nitrogen oxides, indicating that $SO_4^{2-}$ had an inhibitory effect on the adsorption of nitrogen oxides. The further addition of $SO_4^{2-}$ to the $FeS_{10}Zr$ catalyst significantly increased the adsorption of nitrogen oxides at low temperature, but decreased the adsorption of nitrogen oxides at high temperature. When the addition of $SO_4^{2-}$ reached 15%, the adsorption of nitrogen oxides was basically completely suppressed. Because NO can be easily oxidized into $NO_2$ in the presence of $O_2$, and NO together with $NO_2$ are both acidic gases, the addition of $Fe^{3+}$ to the catalyst enhanced its adsorption capacity of nitrogen oxides, while the addition of $SO_4^{2-}$ to the catalyst will inhibited the adsorption capacity of nitrogen oxides. However, due to the synergistic effect between $Fe^{3+}$ and $SO_4^{2-}$, the desorption amount of nitrogen oxides of the $Fe_{3.5}SZr$ catalyst was much less than that of the $Fe_2SZr$ catalyst.

### 3.7 *In situ* diffuse reflectance infrared Fourier transform spectroscopy (DRIFTS)

**3.7.1 $NH_3$ species adsorbed on the different catalysts.** Fig. 7(a) shows the infrared spectra of a series of catalysts containing 5% $SO_4^{2-}$ and different amounts of $Fe^{3+}$ with the saturated adsorption of $NH_3$ at 30 °C and after purging with $N_2$. According to the different reports in the literature and the comparative analysis,[26] the region of 3400–2800 $cm^{-1}$ should be

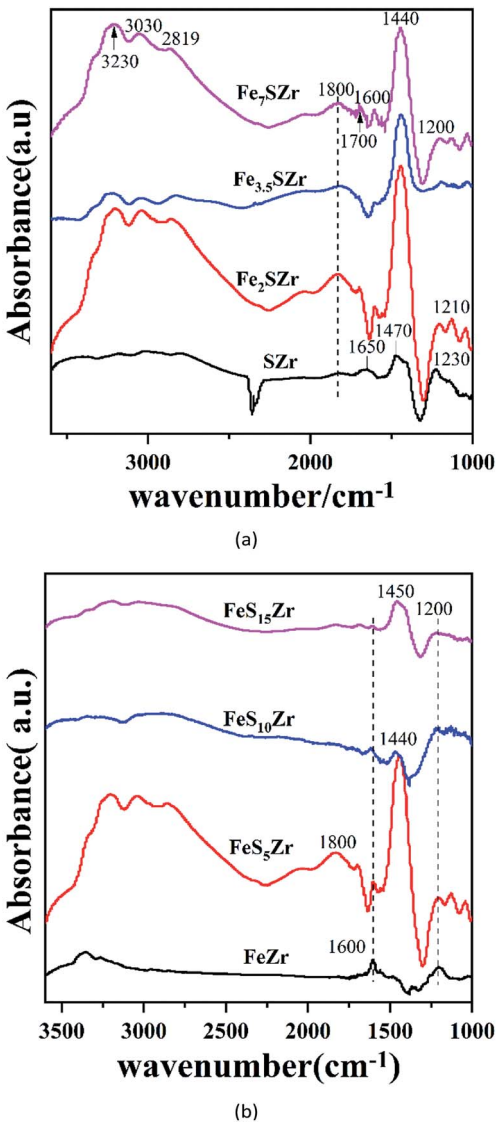


Fig. 7 Infrared spectra of a series of catalysts with the saturated adsorption of $NH_3$ at 30 °C and after purging with $N_2$: (a) catalysts containing 5% $SO_4^{2-}$ and $x$% $Fe^{3+}$ ($x = 0$, 2, 3.5, 7) and (b) catalysts containing 3.5% $Fe^{3+}$ and $y$% $SO_4^{2-}$ ($y = 0$, 5, 10, 15).

Open Access Article. Published on 10 Novemba 2020. Downloaded on 27/04/2026 23:59:39.
This article is licensed under a Creative Commons Attribution-NonCommercial 3.0 Unported Licence.

responsible for the NH stretching vibration, which can be considered as the coordination adsorption formed between $NH_3$ and the oxygen atoms of the metal oxide on the catalyst surface by hydrogen bonding. The absorption at 1600 $cm^{-1}$ is the antisymmetric stretching vibration absorption peak of the $NH_3$ species adsorbed at the Lewis acid sites, while the peaks at 1230, 1210 and 1200 $cm^{-1}$ are attributed to the symmetric stretching vibration absorption peaks of the $NH_3$ species adsorbed at the Lewis acid sites. The peaks at 1440, 1470, 1650, and 1700 $cm^{-1}$ are attributed to the anti-symmetric and symmetric stretching vibration absorption peaks of the $NH_4^+$ species adsorbed at the Brönsted acid sites.[33] It is worth noting that the absorption peak at 1800 $cm^{-1}$ is not attributed to the absorption of $NH_3$ or $NH_4^+$ with an increase in the amount of $Fe^{3+}$. The increase in the amount of $Fe^{3+}$ led to the anti-symmetric stretching vibration absorption peak of the $NH_3$ species adsorbed at the Lewis acid sites. Simultaneously, we found that with a further increase in the amount of $Fe^{3+}$, the amount of $NH_4^+$ species adsorbed at the Brönsted acid sites first increased and then decreased. As shown in Fig. 7(b), the increase in the amount of $SO_4^{2-}$ significantly increased the anti-symmetric and symmetric stretching vibration absorption peaks of the $NH_4^+$ species adsorbed at the Brönsted acid sites, but a further increase in the amount of $SO_4^{2-}$ did not continue to increase the $NH_4^+$ species adsorbed at the Brönsted acid sites, which decreased instead, and this may be due to the synergistic effect of iron and $SO_4^{2-}$.

**3.7.2 The $NO_x$ species adsorbed on the surfaces of the different catalysts.** Fig. 8(a) shows the infrared spectra of a series of catalysts containing 5% $SO_4^{2-}$ and different amounts of $Fe^{3+}$ with the saturated adsorption of NO + $O_2$ at 30 °C and after purging with $N_2$. At 30 °C, the nitrogen oxide vibration absorption peaks appeared at 1630, 1560, 1440, 1280, 1260 and 1240 $cm^{-1}$. According to the literature,[34–37] the vibration absorption peaks at 1630 and 1560 $cm^{-1}$ are attributed to the vibration absorption of the bridged and bidentate nitrate species adsorbed on the catalyst, respectively, and the vibration absorption peaks at 1440, 1280, 1260 and 1240 $cm^{-1}$ are attributed to the linear nitrate species adsorbed on the catalyst. With the addition of $Fe^{3+}$, the vibration absorption peak of the linear nitrate species at 1440 $cm^{-1}$ increased, and the anti-symmetric and symmetric vibration absorption peaks of nitrogen oxides at 1230 $cm^{-1}$ disappeared, showing that the linear nitrate species adsorbed at 1260 $cm^{-1}$. Combined with the NO-TPD results, with the addition of $Fe^{3+}$, the catalyst could readily adsorb the unstable nitrate species (*e.g.*, linear nitrates), and the desorption temperatures of all the adsorbed nitrates shifted towards a lower temperature. Fig. 8(b) shows the infrared spectra of a series of catalysts containing 3.5% $Fe^{3+}$ and different amounts of $SO_4^{2-}$ with the saturated adsorption of NO + $O_2$ at 30 °C and after purging with $N_2$. With the addition of $SO_4^{2-}$ to the catalyst, the $NO_2$ species (1620 $cm^{-1}$) and the linear nitrate species (1280 $cm^{-1}$) on the catalyst surface were reduced, and the vibration absorption peak of the nitrate species showed a red-shift (from 1520 $cm^{-1}$ to 1580 $cm^{-1}$), with a stable nitrate species appearing at 1440 $cm^{-1}$. The addition of $SO_4^{2-}$ inhibited the adsorption of nitrogen oxides on the catalyst, which is consistent with the $NO_x$-TPD results.

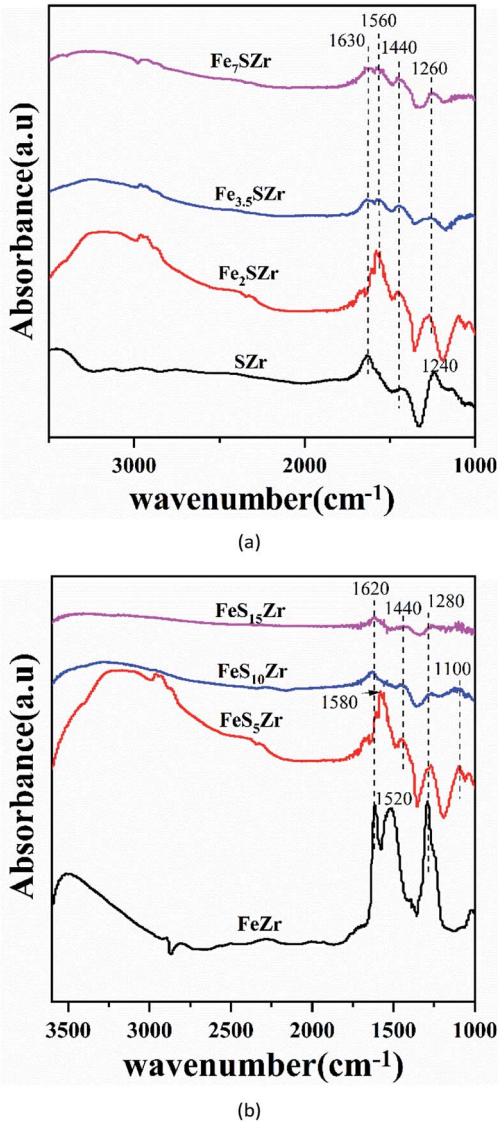


Fig. 8 Infrared spectra of a series of catalysts with the saturated adsorption of NO + $O_2$ at 30 °C and after purging with $N_2$: (a) shows catalysts containing 5% $SO_4^{2-}$ and *x*% $Fe^{3+}$ (*x* = 0, 2, 3.5, 7) and (b) catalysts containing 3.5% $Fe^{3+}$ and *y*% $SO_4^{2-}$ (*y* = 0, 5, 10, 15).

**3.7.3 Transient DRIFTS for the $Fe_7S_5Zr$ and $Fe_2S_{15}Zr$ catalysts.** To better understand the SCR reaction on the sulphated catalysts at high temperature and comparatively analyse the effects of additional $Fe^{3+}$ and $SO_4^{2-}$ on the mechanism of the $NH_3$-SCR catalytic reaction, we investigated the transient DRIFTS for the $Fe_7SZr$ and $FeS_{15}Zr$ catalysts.

*3.7.3.1 Transient DRIFTS of the surface of the $Fe_7SZr$ catalyst at 300 °C.* Fig. 9(a) shows the profile of the time-dependent changes of the adsorbed species on the surface of the $Fe_7SZr$ catalyst at 300 °C after introducing $NH_3$ with the saturated adsorption of NO + $O_2$. Accordingly, after the adsorption of NO + $O_2$ on the catalyst surface was saturated, the adsorption peaks appeared at 1620, 1370 and 1140 $cm^{-1}$. The surface of the catalyst was mainly covered by $NO_2$ species (1620 $cm^{-1}$) and nitrate species (1370 and 1140 $cm^{-1}$).[38] After $NH_3$ was

 This journal is © The Royal Society of Chemistry 2020

Open Access Article. Published on 10 Novemba 2020. Downloaded on 27/04/2026 23:59:39.
This article is licensed under a Creative Commons Attribution-NonCommercial 3.0 Unported Licence.

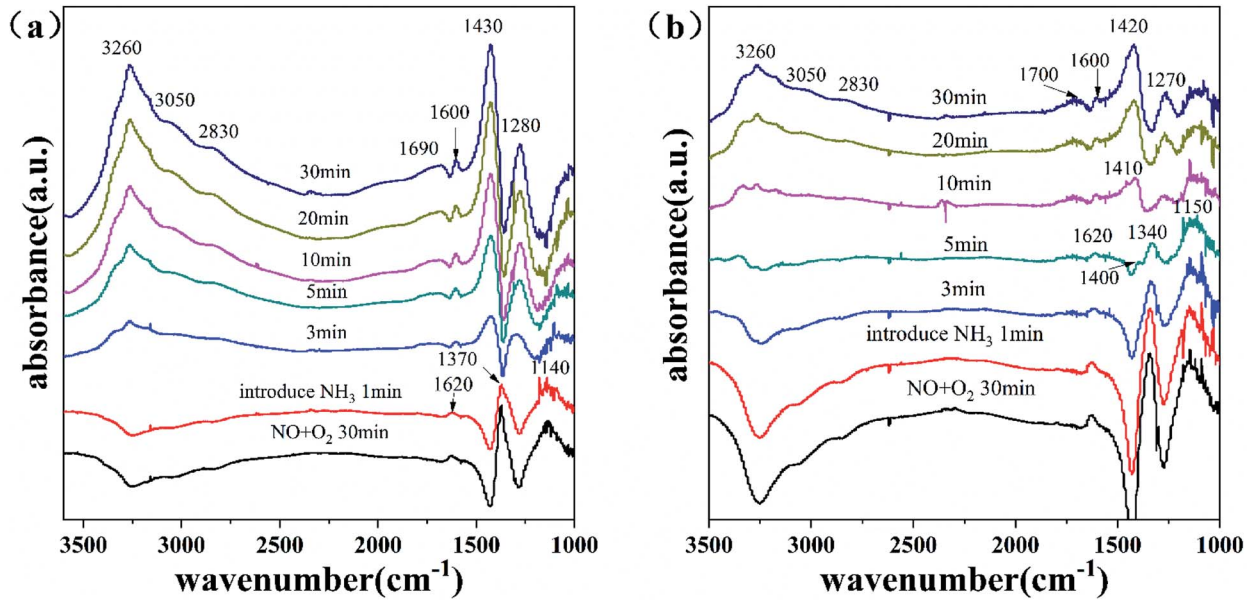


Fig. 9 Profile of the time-dependent changes of the adsorbed species on the surface of different catalysts at 300 °C after introducing $NH_3$ with the saturated adsorption of NO + $O_2$ on the (a) $Fe_7SZr$ catalyst and (b) $FeS_{15}Zr$ catalyst.

introduced for 1 min, the adsorbed nitrogen oxide species began to decrease. After 3 min, the absorption peaks of the adsorbed nitrogen oxide species disappeared, and the adsorption peak attributed to the $NH_4^+$ species at 1430 $cm^{-1}$ appeared, together with the absorption peaks for $NH_3$ (1280 and 1600 $cm^{-1}$) and $NH_4^+$ (1410 and 1690 $cm^{-1}$) species. After 10 min, the absorption peak of $NH_4^+$ on the surface of the catalyst gradually increased. These results indicate that the nitrogen oxide species adsorbed on the $Fe_7SZr$ catalyst surface can react rapidly with $NH_3$ in the gas phase.

Fig. 10(a) shows the profile of the time-dependent changes of the adsorbed species on the surface of the $Fe_7SZr$ catalyst at 300 °C after introducing NO + $O_2$ with the saturated adsorption of $NH_3$. When the $NH_3$ adsorption was saturated, the vibration absorption peaks of $NH_3$ (1280 $cm^{-1}$) and $NH_4^+$ (1680 and 1430 $cm^{-1}$) on the surface of the catalyst appeared. When NO + $O_2$ was introduced onto the catalyst surface, the absorption peak of the ammonia species on the surface of the catalyst did not change significantly. After 5 min, the intensities of all the absorption peaks of the adsorbed $NH_3$ species began to weaken, and even after 30 min, the adsorbed $NH_3$ species had not reacted completely, and the absorption peak of nitrogen oxide did not appear. This demonstrated that the introduction of NO + $O_2$ caused a weak reaction with various types of adsorbed $NH_3$ species on the surface of the catalyst. Thus, combined with Fig. 10(a) and 9(a), at 300 °C the nitrogen oxides adsorbed on the surface of the $Fe_7SZr$ catalyst were the main components that reacted very rapidly with $NH_3$ in the gaseous state, and the various $NH_3$ species adsorbed on the surface could also slowly participate in the reaction.

*3.7.3.2 Transient DRIFTS of the surface of the $FeS_{15}Zr$ catalyst at 300 °C.* Fig. 9(b) shows the profile of the time-dependent changes of the adsorbed species on the surface of the $FeS_{15}Zr$ catalyst at 300 °C after introducing $NH_3$ with the saturated adsorption of NO + $O_2$. Accordingly, after the adsorption of NO + $O_2$ on the catalyst surface was saturated, the adsorption peaks appeared at 1620, 1340 and 1150 $cm^{-1}$. The surface of the catalyst was mainly covered by $NO_2$ species (1620 $cm^{-1}$) and nitrate species (1340 and 1150 $cm^{-1}$).[39] After $NH_3$ was introduced, the adsorbed nitrogen oxides species were gradually weakened in 5 min. At the beginning of the 5th minute, the adsorption peak attributed to the $NH_4^+$ species appeared at 1400 $cm^{-1}$. At the 10th minute, the absorption peaks of the nitrogen oxide species basically disappeared, and the absorption peaks of $NH_3$ (1270 and 1600 $cm^{-1}$) and $NH_4^+$ (1410 and 1700 $cm^{-1}$) species appeared. After 10 min, the catalyst surface was covered by various ammonia species, and they gradually increased. These results indicate that the nitrogen oxide species adsorbed on the surface of the $FeS_{15}Zr$ catalyst can react with $NH_3$ in the gas phase.

Fig. 10(b) shows the profile of the time-dependent changes of the adsorbed species on the surface of the $FeS_{15}Zr$ catalyst at 300 °C after introducing NO + $O_2$ with the saturated adsorption of $NH_3$. After NO + $O_2$ was introduced on the catalyst surface for 5 min, all the adsorbed $NH_3$ species disappeared. Starting from the 10th minute, the surface was gradually occupied by nitrate. This indicates that NO + $O_2$ can react with the various $NH_3$ species adsorbed on the surface. Thus, combined with Fig. 10(b) and 9(b), at 300 °C the $NH_3$ species adsorbed on the surface of the $FeS_{15}Zr$ catalyst can rapidly react with $NO_x$ in the gas phase, while the nitrogen oxide species adsorbed on the surface can also rapidly react with $NH_3$ in the gas phase.

Combined with the results of the DRIFTs study of the transient reactions of the $Fe_7SZr$ and $FeS_{15}Zr$ catalysts at 300 °C, it can be concluded that there are two $NH_3$-SCR reaction paths on the surface of the sulphated iron-based catalyst at 300 °C, namely a Langmuir–Hinshelwood[15] reaction mechanism and an Eley–Rideal[27,33] reaction mechanism, that is,

Open Access Article. Published on 10 Novemba 2020. Downloaded on 27/04/2026 23:59:39.
This article is licensed under a Creative Commons Attribution-NonCommercial 3.0 Unported Licence.

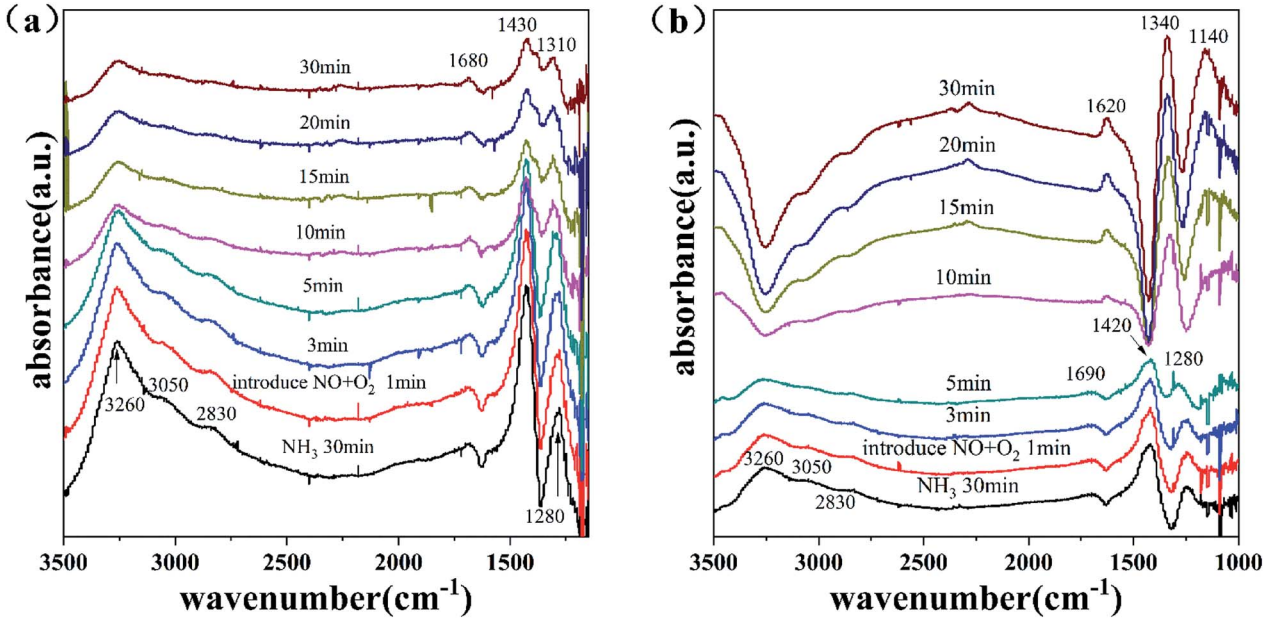


Fig. 10 Profile of the time-dependent changes of the adsorbed species on the surface of different catalysts at 300 °C after introducing NO + $O_2$ with the saturated adsorption of $NH_3$ on the (a) $Fe_7SZr$ catalyst and (b) $FeS_{15}Zr$ catalyst.

$NH_3$ adsorption on the catalyst surface. NO is first oxidized into $NO_2$ to be adsorbed on the surface of the catalyst to produce nitrates or nitrite species, and the $NH_3$ species adsorbed on the surface can react with both gaseous $NO_x$ and the adsorbed $NO_x$ species to produce $N_2$ and $H_2O$. The nitrogen oxide species adsorbed on the surface of the $Fe_7SZr$ catalyst can react very rapidly with the gaseous $NH_3$, while various $NH_3$ species adsorbed on the surface can also slowly participate in the reaction, indicating that when the amount of $Fe_2O_3$ in the catalyst increases, the SCR reaction occurring on the catalyst obviously follows the Langmuir–Hinshelwood reaction path, with a small portion of the reaction following the Eley–Rideal reaction mechanism simultaneously. The $NH_3$ species adsorbed on the surface of the $FeS_{15}Zr$ catalyst at 300 °C can rapidly react with the $NO_x$ in the gas phase, and the nitrogen oxides species adsorbed on the surface can also rapidly react with the $NH_3$ in the gas phase. This indicates that when the amount of $SO_4^{2-}$ in the catalyst increases, the SCR reaction on the surface of the catalyst obviously follows the Eley–Rideal reaction mechanism, mainly because the increase in the amount of $SO_4^{2-}$ significantly enhances the ammonia adsorption capacity of the catalyst at a high temperature, while reducing the adsorption of nitrogen oxides, which is conducive to enhancing the $NH_3$ adsorption by the catalyst, thereby promoting the SCR reaction at high temperature. This is consistent with the results of the activity test for the catalyst with varying amounts of $SO_4^{2-}$.

## 4. The synergistic mechanism of $Fe^{3+}$ and sulphates for $NH_3$-SCR

The roles of $Fe^{3+}$ and sulphates were very different at low temperature and high temperature. When the $SO_4^{2-}$ content is constant, the addition of $Fe^{3+}$ to the catalyst will enhance its adsorption capacity of nitrogen oxides and $NH_3$ species at moderate and low temperatures. According to the references,[27,33,40,41] the mechanism of the SCR generally follows the Langmuir–Hinshelwood reaction path at moderate and low temperatures, and thus the $Fe^{3+}$ obviously adsorbed $NH_3$ and oxidized it to $-NH_2$, which is the important intermediate species for the SCR reaction[42–46] and can react with the NO oxidation species ($NO_2^-$ and $NO_3^-$) to form the intermediate species, and then decompose to $N_2$ and $H_2O$. Thus, the addition of $Fe^{3+}$ improved the redox ability, which affected the activity for the SCR at moderate and low temperatures. However, at high temperature, an increase in the amount of $Fe^{3+}$ will promote the oxidation of $NH_3$ because it can increase the redox activity of the catalyst, which results in a decrease in the efficiency of the catalytic reduction of nitrogen oxides. When the content of $Fe^{3+}$ is constant, with an increase in the content of $SO_4^{2-}$, the concentration of $Fe^{3+}$ on the surface showed a decreasing trend because of the formation of $Fe_2(SO_4)_3$, which leads to the complete inhibition of the adsorption of $NO_x$ and $NH_3$ to reduce the conversion of $NO_x$ in $NH_3$-SCR at moderate and low temperature. At high temperature, the redox activity of the catalyst is reduced with the addition of $SO_4^{2-}$, which restrains the oxidation reaction of $NH_3$ on the catalyst. Meanwhile, the significant increase in $NH_4^+$ species adsorbed at the Brönsted acid sites improves the activity for the SCR, which follows the Eley–Rideal reaction path. Overall, the effect on the SCR for $Fe^{3+}$ and $SO_4^{2-}$ was restrained by each of them, and thus only the appropriate contents of $Fe^{3+}$ and $SO_4^{2-}$ could result in high activity in the temperature range of 300–450 °C. Similar to oxide catalysts such as Mo–Fe,[47] W–Fe,[48] W–Ce,[49] and Mo–Fe[50] oxides, the sulphated iron-based catalysts possess acid-redox dinuclear sites, where $Fe^{3+}$ is the redox site and $SO_4^{2-}$ is the acid site. The

 This journal is © The Royal Society of Chemistry 2020

Open Access Article. Published on 10 Novemba 2020. Downloaded on 27/04/2026 23:59:39.
This article is licensed under a Creative Commons Attribution-NonCommercial 3.0 Unported Licence.

interfaces of the acid-redox sites are key to the SCR reaction activities. Thus, designing catalysts to optimize the interaction between the acid-redox sites is an effective measure to control NO emissions.

## 5. Conclusions

Different sulphated iron-based catalysts with various loadings of $Fe^{3+}$ and $SO_4^{2-}$ on $ZrO_2$ were prepared *via* the incipient wetness method, and investigated for the selective catalytic reduction (SCR) of $NO_x$ by ammonia. Compared to all the catalysts, the $Fe_2SZr$ catalyst could achieve above 90% $NO_x$ removal efficiency at 350–450 °C, and the main reactions on its surface were the $NH_3$-SCR reaction and the oxidation of $NH_3$. Meanwhile, the interaction between $Fe^{3+}$ and $SO_4^{2-}$ was found to affect the redox ability, acid sites, adsorption of $NO_x$ and $NH_3$, and play a role in the SCR activity. Specifically, increasing the content of $Fe^{3+}$ improved the redox activity of the catalyst and enhanced the adsorption of ammonia at medium and low temperatures. In addition, increasing the amount of $Fe^{3+}$ promoted the oxidation of $NH_3$ at high temperatures, which led to a reduction in the efficiency of $NO_x$ conversion. With an increase in $SO_4^{2-}$, the concentration of $Fe^{3+}$ on the surface of the catalyst showed a decreasing trend because of the formation of $Fe_2(SO_4)_3$, which inhibited the adsorption of $NO_x$ and $NH_3$ and reduced the $NO_x$ conversion of the $NH_3$-SCR at medium and low temperatures. At high temperatures, the addition of $SO_4^{2-}$ reduced the redox activity of the catalyst and inhibited the oxidation reaction of $NH_3$. Meanwhile, the significant increase in $NH_4^+$ species adsorbed on the Brönsted acid sites improved the SCR activity because the main reaction pathway over the $Fe_xS_yZr$ catalyst follows the Eley–Rideal mechanism at high temperatures.

## Conflicts of interest

There are no conflicts to declare.

## Acknowledgements

This work was financially supported by the National High-Tech Research and Science and Technology Plan Program of Hebei Province (Grant No. 206Z3702G) and Development (Air Pollution Control Technology Research) Program of China (Grant No. 2016YFC0205302 and No. 2016YFC0205300) and National Natural Science Fund of China (Grant No. 21507100).

## References

1 Z. Fu, M. Guo, C. Liu, N. Ji, C. Song and Q. Liu, Design and Synthesis Functional Selective Catalytic Reduction Catalyst for NOx Removal, *Procedia Eng.*, 2015, **121**, 952–956.
2 M. Jabłońska and R. Palkovits, Copper based catalysts for the selective ammonia oxidation into nitrogen and water vapour—Recent trends and open challenges, *Appl. Catal., B*, 2016, **181**, 332–351.
3 G. Busca, L. Lietti, G. Ramis and F. Berti, Chemical and mechanistic aspects of the selective catalytic reduction of NOx by ammonia over oxide catalysts: a review, *Appl. Catal., B*, 1998, **18**, 1–36.
4 A. Boubnov, H. W. P. Carvalho, D. E. Doronkin, T. Guenter, E. Gallo, A. J. Atkins, C. R. Jacob and J. D. Grunwaldt, Selective Catalytic Reduction of NO Over Fe-ZSM-5: Mechanistic Insights by Operando HERFD-XANES and Valence-to-Core X-ray Emission Spectroscopy, *J. Am. Chem. Soc.*, 2014, **136**, 13006–13015.
5 D. Jo, G. T. Park, T. Ryu and S. B. Hong, Economical synthesis of high-silica LTA zeolites: a step forward in developing a new commercial NH3-SCR catalyst, *Appl. Catal., B*, 2019, **243**, 212–219.
6 J. Mu, X. Li, W. Sun, S. Fan, X. Wang, L. Wang, M. Qin, G. Gan, Z. Yin and D. Zhang, Inductive Effect Boosting Catalytic Performance of Advanced Fe1–xVxOδ Catalysts in Low-Temperature NH3 Selective Catalytic Reduction: Insight into the Structure, Interaction, and Mechanisms, *ACS Catal.*, 2018, **8**, 6760–6774.
7 P. Fabrizioli, T. Bürgi and A. Baiker, Environmental Catalysis on Iron Oxide–Silica Aerogels: Selective Oxidation of NH3 and Reduction of NO by NH3, *J. Catal.*, 2002, **206**, 143–154.
8 S. Ding, F. Liu, X. Shi and H. Hong, Promotional effect of Nb additive on the activity and hydrothermal stability for the selective catalytic reduction of NOx with NH3 over CeZrOx catalyst, *Appl. Catal., B*, 2016, **180**, 766–774.
9 C. Sun, H. Liu, W. Chen, D. Chen, S. Yu, A. Liu, L. Dong and S. Feng, Insights into the Sm/Zr co-doping effects on N2 selectivity and SO2 resistance of a MnOx-TiO2 catalyst for the NH3-SCR reaction, *Chem. Eng. J.*, 2018, **347**, 27–40.
10 S. Yang, F. Qi, S. Xiong, D. Hao and J. Li, MnOx supported on Fe-Ti spinel: a novel Mn based low temperature SCR catalyst with a high N2 selectivity, *Appl. Catal., B*, 2016, **181**, 570–580.
11 R. Zhang, Y. Li and T. Zhen, Ammonia selective catalytic reduction of NO over Fe/Cu-SSZ-13, *RSC Adv.*, 2014, **4**, 52130–52139.
12 F. Cao, S. Su, J. Xiang, P. Wang, S. Hu, L. Sun and A. Zhang, The activity and mechanism study of Fe-Mn-Ce/γ-Al_2O_3 catalyst for low temperature selective catalytic reduction of NO with NH_3, *Fuel*, 2015, **139**, 232–239.
13 B. Shen, T. Liu, N. Zhao and X. Yang, Iron-doped Mn-Ce/TiO2 catalyst for low temperature selective catalytic reduction of NO with NH3, *J. Environ. Sci.*, 2010, **22**, 1447–1454.
14 W. Zhao, C. Li, P. Lu, Q. Wen, Y. Zhao, X. Zhang, C. Fan and S. Tao, Iron, lanthanum and manganese oxides loaded on γ-Al2O3 for selective catalytic reduction of NO with NH3 at low temperature, *Environ. Technol.*, 2013, **34**, 81–90.
15 G. Zhou, B. Zhong, W. Wang, X. Guan, B. Huang, D. Ye and H. Wu, In situ DRIFTS study of NO reduction by NH3 over Fe–Ce–Mn/ZSM-5 catalysts, *Catal. Today*, 2011, **175**, 157–163.
16 Y. Xia, W. Zhan, Y. Guo, Y. Guo and G. Lu, Fe-Beta zeolite for selective catalytic reduction of NOx with NH3: influence of Fe content, *Chin. J. Catal.*, 2016, **37**, 2069–2078.
17 Z. Ma, H. Yang, L. Qian, J. Zheng and X. Zhang, Catalytic reduction of NO by NH3 over Fe–Cu–OX/CNTs-TiO2

Open Access Article. Published on 10 Novemba 2020. Downloaded on 27/04/2026 23:59:39.
This article is licensed under a Creative Commons Attribution-NonCommercial 3.0 Unported Licence.

composites at low temperature, *Appl. Catal., A*, 2012, **427–428**, 43–48.

18 T. Gu, L. Yue, X. Weng, H. Wang and Z. Wu, The enhanced performance of ceria with surface sulfation for selective catalytic reduction of NO by NH3, *Catal. Commun.*, 2010, **12**, 310–313.

19 M. Lei, J. Li, K. Rui and L. Fu, Catalytic Performance, Characterization, and Mechanism Study of Fe2(SO4)3/TiO2 Catalyst for Selective Catalytic Reduction of NOx by Ammonia, *J. Phys. Chem. C*, 2011, **115**, 7603–7612.

20 H. Zhang, Y. Zou and Y. Peng, Influence of sulfation on CeO2-ZrO2 catalysts for NO reduction with NH3, *Chin. J. Catal.*, 2017, **38**, 160–167.

21 Q. Lu, W. Yun, D. Pang, O. Feng and C. Zhang, SO42–Mn-Co-Ce supported on TiO2/SiO2 with high sulfur durability for low-temperature SCR of NO with NH3, *Catal. Commun.*, 2016, **78**, 22–25.

22 Q. Zhang, J. Zhang, Z. Song, N. Ping and L. Xin, A novel and environmentally friendly SO42–/CeO2 catalyst for the selective catalytic reduction of NO with NH3, *J. Ind. Eng. Chem.*, 2016, **34**, 165–171.

23 Y. Yu, J. Chen, J. Wang and Y. Chen, Performances of CuSO4/TiO2 catalysts in selective catalytic reduction of NOx by NH3, *Chin. J. Catal.*, 2016, **37**, 281–287.

24 T. Xu, X. Wu, X. Liu, L. Cao, Q. Lin and D. Weng, Effect of barium sulfate modification on the SO2 tolerance of V2O5/TiO2 catalyst for NH3-SCR reaction, *J. Environ. Sci.*, 2017, **57**, 110–117.

25 X. Du, X. Wang, Y. Chen, X. Gao and L. Zhang, Supported metal sulfates on Ce–TiOx as catalysts for NH3–SCR of NO: high resistances to SO2 and potassium, *J. Ind. Eng. Chem.*, 2016, **36**, 271–278.

26 L. Jian, Z. Zhen, J. Wang, C. Xu, A. Duan, G. Jiang and Q. Yang, The highly active catalysts of nanometric CeO2-supported cobalt oxides for soot combustion, *Appl. Catal., B*, 2008, **84**, 185–195.

27 N. Apostolescu, B. Geiger, K. Hizbullah, M. T. Jan, S. Kureti, D. Reichert, F. Schott and W. Weisweiler, Selective catalytic reduction of nitrogen oxides by ammonia on iron oxide catalysts, *Appl. Catal., B*, 2006, **62**, 104–114.

28 X. Wang, S. Wu, W. Zou, S. Yu and L. Dong, Fe-Mn/Al2O3 catalysts for low temperature selective catalytic reduction of NO with NH3, *Chin. J. Catal.*, 2016, **37**, 1314–1323.

29 S. Yang, C. Liu, H. Chang, L. Ma, Z. Qu, N. Yan, C. Wang and J. Li, Improvement of the Activity of γ-Fe2O3 for the Selective Catalytic Reduction of NO with NH3 at High Temperatures: NO Reduction versus NH3 Oxidization, *Ind. Eng. Chem. Res.*, 2013, **52**, 5601–5610.

30 R. Q. Long and R. T. Yang, Selective Catalytic Oxidation of Ammonia to Nitrogen over Fe2O3–TiO2 Prepared with a Sol–Gel Method, *J. Catal.*, 2002, **207**, 158–165.

31 L. S. Cheng, R. T. Yang and C. Ning, Iron Oxide and Chromia Supported on Titania-Pillared Clay for Selective Catalytic Reduction of Nitric Oxide with Ammonia, *J. Catal.*, 1996, **164**, 70–81.

32 R. Q. Long and R. T. Yang, The promoting role of rare earth oxides on Fe-exchanged TiO 2-pillared clay for selective catalytic reduction of nitric oxide by ammonia, *Appl. Catal., B*, 2000, **27**, 87–95.

33 G. Ramis, L. Yi, G. Busca, M. Turco, E. Kotur and R. J. Willey, Adsorption, Activation, and Oxidation of Ammonia over SCR Catalysts, *J. Catal.*, 1995, **157**, 523–535.

34 A. Bourane, O. Dulaurent, S. Salasc, C. Sarda, C. Bouly and D. Bianchi, Heats of Adsorption of Linear NO Species on a Pt/Al2O3 Catalyst Using in Situ Infrared Spectroscopy under Adsorption Equilibrium, *J. Catal.*, 2001, **204**, 77–88.

35 A. Kotsifa, D. I. Kondarides and X. E. Verykios, Comparative study of the chemisorptive and catalytic properties of supported Pt catalysts related to the selective catalytic reduction of NO by propylene, *Appl. Catal., B*, 2007, **72**, 136–148.

36 W. Schieer, H. Vinek and A. Jentys, Surface species during catalytic reduction of NO by propene studied by in situ IR-spectroscopy over PT supported on mesoporous Al2O3 with MCM-41 type structure, *Appl. Catal., B*, 2001, **33**, 263–274.

37 M. A. Larrubia, G. Ramis and G. Busca, An FT-IR study of the adsorption and oxidation of N-containing compounds over Fe 2O3-TiO2 SCR catalysts, *Appl. Catal., B*, 2001, **30**, 101–110.

38 L. J. France, Q. Yang, W. Li, Z. Chen, J. Guang, D. Guo, L. Wang and X. Li, Ceria modified FeMnOx—Enhanced performance and sulphur resistance for low-temperature SCR of NOx, *Appl. Catal., B*, 2017, **206**, 203–215.

39 T. Venkov, K. Hadjiivanov and D. Klissurski, IR spectroscopy study of NO adsorption and NO + O2 co-adsorption on Al2O3, *Phys. Chem. Chem. Phys.*, 2002, **4**, 2443–2448.

40 J. Liu, X. Li, R. Li, Q. Zhao, J. Ke, H. Xiao, L. Wang, S. Liu, M. Tadé and S. Wang, Facile synthesis of tube-shaped Mn-Ni-Ti solid solution and preferable Langmuir-Hinshelwood mechanism for selective catalytic reduction of NO by NH3, *Appl. Catal., A*, 2018, **549**, 289–301.

41 J. Liu, G.-q. Li, Y.-f. Zhang, X.-q. Liu, Y. Wang and Y. Li, Novel Ce-W-Sb mixed oxide catalyst for selective catalytic reduction of NOx with NH3, *Appl. Surf. Sci.*, 2017, **401**, 7–16.

42 J. Fan, P. Ning, Z. Song, X. Liu, L. Wang, J. Wang, H. Wang, K. Long and Q. Zhang, Mechanistic aspects of NH3-SCR reaction over CeO2/TiO2-ZrO2-SO42– catalyst: in situ DRIFTS investigation, *Chem. Eng. J.*, 2018, **334**, 855–863.

43 J. Zhang, X. Li, P. Chen and B. Zhu, Research Status and Prospect on Vanadium-Based Catalysts for NH(3)-SCR Denitration, *Materials*, 2018, **11**, 1632.

44 J. Liu, R.-t. Guo, M.-y. Li, P. Sun, S.-m. Liu, W.-g. Pan, S.-w. Liu and X. Sun, Enhancement of the SO2 resistance of Mn/TiO2 SCR catalyst by Eu modification: a mechanism study, *Fuel*, 2018, **223**, 385–393.

45 J.-W. Shi, Y. Wang, R. Duan, C. Gao, B. Wang, C. He and C. Niu, The synergistic effects between Ce and Cu in CuyCe1–yW5Ox catalysts for enhanced NH3-SCR of NOx and SO2 tolerance, *Catal. Sci. Technol.*, 2019, **9**, 718–730.

46 H. Wang, P. Ning, Y. Zhang, Y. Ma, J. Wang, L. Wang and Q. Zhang, Highly efficient WO3-FeOx catalysts synthesized using a novel solvent-free method for NH3-SCR, *J. Hazard. Mater.*, 2020, **388**, 121812.

 This journal is © The Royal Society of Chemistry 2020

Open Access Article. Published on 10 Novemba 2020. Downloaded on 27/04/2026 23:59:39.
This article is licensed under a Creative Commons Attribution-NonCommercial 3.0 Unported Licence.

47 Y. Xin, N. Zhang, Q. Li, Z. Zhang, X. Cao, L. Zheng, Y. Zeng and J. A. Anderson, Active Site Identification and Modification of Electronic States by Atomic-Scale Doping To Enhance Oxide Catalyst Innovation, *ACS Catal.*, 2018, **8**, 1399–1404.

48 Z. Liu, H. Su, B. Chen, J. Li and S. I. Woo, Activity enhancement of WO3 modified Fe2O3 catalyst for the selective catalytic reduction of NOx by NH3, *Chem. Eng. J.*, 2016, **299**, 255–262.

49 J. Chen, Y. Chen, M. Zhou, Z. Huang, J. Gao, Z. Ma, J. Chen and X. Tang, Enhanced Performance of Ceria-Based NOx Reduction Catalysts by Optimal Support Effect, *Environ. Sci. Technol.*, 2017, **51**, 473–478.

50 W. Qu, X. Liu, J. Chen, Y. Dong, X. Tang and Y. Chen, Single-atom catalysts reveal the dinuclear characteristic of active sites in NO selective reduction with NH3, *Nat. Commun.*, 2020, **11**, 1532.